


 Cite this: *RSC Adv.*, 2023, **13**, 1867

## Electrochemical behaviour of cellulose/reduced graphene oxide/carbon fiber paper electrodes towards the highly sensitive detection of amitrole

 Hui Hu,<sup>a</sup> Si Wu,<sup>b</sup> Cheng Wang,<sup>c</sup> Xiaohui Wang,<sup>b</sup> and Xiaowen Shi<sup>b</sup>        

Amitrole is a non-selective triazole herbicide that is widespread used to control a variety of weeds in agriculture, but it may pollute the environment and do harm to organisms. Thus, it is of critical significance to enlist a low-cost, sensitive, stable and renewable method to detect amitrole. In this paper, electrochemical experiments were carried out using carbon fibers/reduced graphene oxide/cellulose paper electrodes, which demonstrated good electrocatalytic performance for amitrole detection. The electrochemical process of amitrole on the surface of the reduced paper electrode was a quasi-reversible reaction controlled by diffusion. Cyclic voltammetry and the amperometric *i-t* curve method were used for amitrole determination at a micro molar level and higher-concentration range with the following characteristics: linear range  $5 \times 10^{-6}$  mol L<sup>-1</sup> to  $3 \times 10^{-5}$  mol L<sup>-1</sup>, detection limit  $2.44 \times 10^{-7}$  mol L<sup>-1</sup>. In addition, the relative standard deviation of repeatability is 3.74% and of stability is 4.68%. The reduced paper electrode with high sensitivity, low detection limit, good stability and repeatability provides novel ideas for on-site amitrole detection in food and agriculture.

Received 1st December 2022  
 Accepted 27th December 2022

DOI: 10.1039/d2ra07662d

rsc.li/rsc-advances

### 1. Introduction

Amitrole (3-amino-1,2,4-triazole) is a non-selective triazole herbicide, which is commonly used in combination with other chemical agents to control a variety of weeds in agriculture.<sup>1-4</sup> It is an organic heterocyclic compound that can block the biosynthesis of carotenoid.<sup>5,6</sup> This herbicide has strong polarity, low volatility and high solubility in water, so it may pollute groundwater, surface water and contaminate food through plants, fruit and water medium. Even worse, it will cause toxic side effects and damage human health when it enters the body.<sup>6-8</sup> Traditional strategies and analytical techniques have been developed for the detection of amitrole, such as high performance liquid chromatography (HPLC),<sup>7,9</sup> gas/liquid chromatography-mass spectrometry (GC/LC-MS)<sup>10,11</sup> and capillary electrophoresis.<sup>12,13</sup> However, these methods have their drawbacks with high operation cost,<sup>5</sup> complicated procedure, time-consuming, and requirement of skilled personnel.<sup>14,15</sup> Electrochemical methods have attracted much attention due to

their advantages of simple and convenient operation, cost-effectiveness, precision and rapid analysis and high sensitivity.<sup>16,17</sup> Electrochemistry has unique versatilities, its detection data is easy to read and analyze, and it is suitable for miniaturization, intelligence and field applications to screen and monitor pollutants.<sup>18-20</sup>

In the electrochemical detection of analytes, the working electrode is extremely important.<sup>19</sup> When using electrochemical methods, applying voltage through various electrochemical technologies such as cyclic voltammetry will cause electrochemical redox reaction of analytes on the working electrode.<sup>21</sup> The reaction mechanism and chemical properties of the analytes can be explored by outputting the change of its response current. The working electrodes made of different materials have different properties and have their own advantages in the detection of analytes. When detected on traditional bare electrodes, amitrole has a high oxidation overpotential and will contaminate the electrode.<sup>1</sup> The selectivity of detection is also affected by the coexistence of other interfering molecules with similar oxidation potential.<sup>15</sup> These limitations can be overcome by electrode modification. A literature investigation has shown that different kinds of modified electrodes have been used for the electrochemical detection of amitrole, including metals and their oxides,<sup>3,22,23</sup> phthalocyanine,<sup>2,16,17</sup> labeled enzyme or probe reactions<sup>6,24</sup> and carbon materials,<sup>25,26</sup> etc. These modified electrodes have high sensitivity and good selectivity, but the modification process is complex and time-consuming. In this regard, functionalized paper-based electrodes provide opportunities for low-cost, efficient, and

<sup>a</sup>School of Resource and Environmental Science, Hubei Engineering Center of Natural Polymers-Based Medical Materials, Hubei Biomass-Resource Chemistry and Environmental Biotechnology Key Laboratory, Hubei International Scientific and Technological Cooperation Base of Sustainable Resource and Energy, Wuhan University, Wuhan 430079, China. E-mail: shixw@whu.edu.cn

<sup>b</sup>College of Resources and Environmental Engineering, Hubei Key Laboratory for Efficient Utilization and Agglomeration of Metallurgic Mineral Resources, Wuhan University of Science and Technology, Wuhan 430081, China

<sup>c</sup>State Key Laboratory of Pulp and Paper Engineering, South China University of Technology, Guangzhou 510640, China



environmentally friendly stable chemical analysis.<sup>27,28</sup> At present, a variety of paper-based electrochemical sensors have been developed for environmental field monitoring,<sup>29</sup> rapid analysis of food safety,<sup>30</sup> biomedical detection,<sup>31</sup> but there are few examples of pesticide detection in literature reports.<sup>14,32</sup>

Cellulose-based paper has attracted considerable attention due to environmentally friendly and degradability of the cellulose substrate.<sup>33,34</sup> Graphene has high specific surface area, excellent electrochemical performance and thin-layer nano-structure, which is a good catalyst support.<sup>19,35</sup> In our previous work, a composite paper electrode made from carbon fibers (CF), graphene oxide (GO) and cellulose fibers was fabricated in large scale with superior electrocatalytic property.<sup>28</sup> To expand the electrochemical application of the CF/GO/cellulose paper electrode, we selected this composite paper electrode for amitrole detection. As far as we know, this work is the first report on amitrole detection by using paper electrode, which is low-cost, simple, fast and efficient, and environmentally friendly. We explored the electrochemical reaction type, detection range and detection limit of amitrole by cyclic voltammetry and amperometric *i*-*t* method. In addition, the interference experiment and real sample detection were carried out. The results show that the CF/GO/cellulose paper electrode has the potential to electrochemical detection of pesticides with portable and disposable manner, which provides novel ideas for on-site amitrole detection in food and agriculture.

## 2. Experimental

### 2.1. Materials

Amitrole was obtained from Sigma. The carbon fibers/graphene oxide/cellulose paper electrochemical sensors were received from State Key Laboratory of Pulp and Paper Engineering, South China University of Technology (SCUT). The 0.1 mol L<sup>-1</sup> phosphate buffer (PB) used as the supporting electrolyte was prepared with appropriate amounts of Na<sub>2</sub>HPO<sub>4</sub>·12H<sub>2</sub>O and NaH<sub>2</sub>PO<sub>4</sub>·2H<sub>2</sub>O, and the pH adjusted with 0.1 M H<sub>3</sub>PO<sub>4</sub> or NaOH. Ultrapure water of resistivity 18.2 M was obtained from a Molgene and was used throughout the experiments. All the experiments were carried out at room temperature. All other reagents were analytical reagent grade and were used as received without further purification.

### 2.2. Instrumentation

Electrochemical experiments were recorded using a three electrode system controlled by CHI 840D electrochemical workstation (Shanghai, China), with a CF/GO/cellulose composite paper (1 × 1.5 cm) as a working electrode, an Ag/AgCl reference electrode and a platinum counter electrode. The surfaces of the paper-based electrodes were characterized by scanning electron microscope (SEM).

### 2.3. Electrochemical measurements

**2.3.1 Electrochemical reduction of GO.** Graphene oxide (GO) of the CF/GO/cellulose paper was electrochemically reduced by amperometric *i*-*t* curve (*I*-*t*) using a three-electrode

system, the electrolyte was 1 M KCl solution, the reaction condition was -0.9 V, and the reaction time was 1000 s.<sup>28</sup>

**2.3.2 Electrochemical sensing.** The electrochemical performance of paper electrode under different parameters was studied by cyclic voltammetry (CV) and amperometric *i*-*t* curve (*I*-*t*). Electrochemical experiments were performed using a three-electrode system and the electrolyte was 0.1 M PB. The parameters for the CV were: a potential range between -0.8 V and +0.8 V; the scan rate was varied from 5–500 mV s<sup>-1</sup>. The applied potentials for the *I*-*t* were: +0.45 V/+0.50 V/+0.55 V and run time was varied with concentration range.

## 3. Results and discussion

### 3.1. Characterization of CF/GO/cellulose paper electrode

The composite paper is composed of carbon fibers (CF), graphene oxide (GO) and cellulose, wherein the mass ratio of CF and cellulose is 1 : 1, and the content of GO is 8% (w/w).<sup>28</sup> CF can impart conductivity to paper electrodes, GO endow them with electrocatalytic activity. The composite paper is uniform, stable and foldable. As shown in Fig. 1a, the composite paper (25 cm in diameter) can be cut into desired shapes to facilitate the experiment. Fig. 1b shows the rectangular sheets (1 × 1.5 cm), which were used as working electrodes in subsequent experiments by clamping them with electrode clips. Then, we observed the surface microstructure of the paper electrode using scanning electron microscopy (SEM). Fig. 1c shows that the surface microscopy of the paper electrode is relatively uniform, which is interwoven by cellulose/GO and CF, while GO covers on the surface of cellulose.

It is reported that reduction of GO in the paper electrode has a significant impact on electrochemical detection.<sup>28</sup> Thus, the CF/GO/cellulose paper electrode was reduced at -0.9 V for 1000 s. The functional groups of the GO paper electrode before and after the reduction were studied by FTIR spectroscopy. As shown in Fig. 1d, the strong peak at 3450 cm<sup>-1</sup> from the stretching vibration of O-H group, the bonds at 2980 cm<sup>-1</sup> and 2910 cm<sup>-1</sup> are attributed to C-H stretching and the peak at 1640 cm<sup>-1</sup> corresponded to the skeletal vibration of the C=O stretch.<sup>36</sup> For the GO paper electrode, characteristic peaks corresponding to various functional groups, including C-O (1120 cm<sup>-1</sup>, 1050 cm<sup>-1</sup>), C-OH (1310 cm<sup>-1</sup>).<sup>37,38</sup> After the GO is electrochemically reduced, the broad O-H stretching bond and the C=O bond remain, but the intensity of the oxygen functionalities C-O bond at 1050 cm<sup>-1</sup> was markedly weakened, indicating that part of GO was reduced to rGO.

### 3.2. Electrochemical performance of CF/rGO/cellulose paper electrode

**3.2.1 Electrocatalytic characterization of reduced paper electrode.** The effective sensing surface area of the paper electrode was determined using cyclic voltammetry (Fig. 2a) on the [Fe(CN)<sub>6</sub>]<sup>3-/-4-</sup> redox system and applying the Randles–Sevcik eqn (1):<sup>39</sup>

$$I_p = (2.69 \times 10^5) n^{3/2} A D^{1/2} C v^{1/2} \quad (1)$$



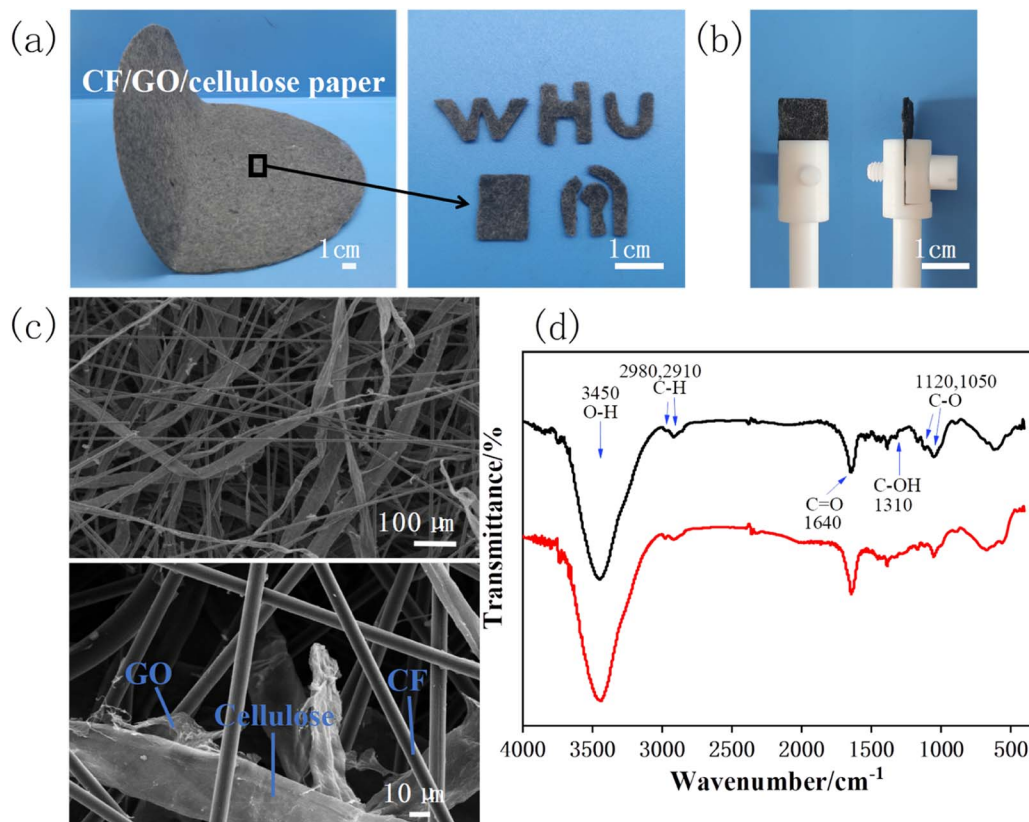


Fig. 1 (a) The appearance of CF/GO/cellulose paper (diameter is 25 cm) and it was cut into different shapes. (b) Working electrodes: 1 × 1.5 cm paper slices. (c) Surface microstructure of the GO paper electrode by SEM. (d) FTIR spectra: the upper curve shows GO paper electrode and the lower curve shows reduced GO paper electrode.

where  $I_p$  is the anodic peak current (A),  $n$  is the number of electrons transferred,  $A$  is the effective sensing surface area ( $\text{cm}^2$ ),  $D$  is the diffusion coefficient of  $[\text{Fe}(\text{CN})_6]^{3-/-4-}$  ( $\text{cm}^2 \text{ s}^{-1}$ ),  $C$  is the bulk concentration of redox probe ( $\text{mol cm}^{-3}$ ), and  $v$  is the scan rate ( $\text{V s}^{-1}$ ). The  $D$  and  $n$  values for  $[\text{Fe}(\text{CN})_6]^{3-/-4-}$  were  $7.6 \times 10^{-6} \text{ cm}^2 \text{ s}^{-1}$  at  $25^\circ\text{C}$  (ref. 40) and 1 respectively.

Experiments at different scan rates were performed in a solution of 1 mM  $\text{K}_3[\text{Fe}(\text{CN})_6]$  in 1 M KCl. The plot of  $I_p$  vs.  $v^{1/2}$  (Fig. 2b) was found to be linear with the slope of 70.88 and

136.67 for the paper electrode (PE) and the reduced paper electrode (rPE) respectively regarding following equations:

$$\text{PE: } I_p (1 \times 10^{-4} \text{ A}) = 70.88v^{1/2} (\text{V s}^{-1}) - 0.549; R^2 = 0.999$$

$$\text{rPE: } I_p (1 \times 10^{-4} \text{ A}) = 136.67v^{1/2} (\text{V s}^{-1}) - 5.018; R^2 = 0.999$$

The effective sensing surface areas were estimated to be  $9.56 \text{ cm}^2$  for PE and  $18.43 \text{ cm}^2$  for rPE. Therefore, rPE is

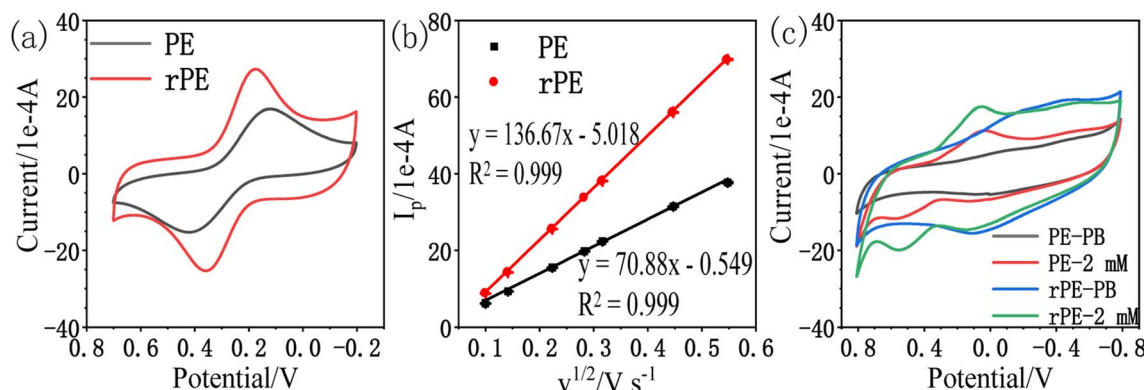


Fig. 2 (a) CVs of the paper electrodes in 1 mM  $\text{K}_3[\text{Fe}(\text{CN})_6]$  in 1 M KCl. Scan rate = 50 mV s⁻¹. (b) Plots of oxidation peak current ( $I_p/1 \times 10^{-4} \text{ A}$ ) vs. square root of the scan rate ( $v^{1/2}$ ) for PE and rPE. (c) CVs of PB (pH 7) and 2 mM amitrole. Scan rate = 50 mV s⁻¹.



expected to perform better than PE based on the effective electrode area. The peak potential separation ( $\Delta E$ ) can reflect the electron transfer ability, which is used to evaluate the electrode surface performance as an electrocatalytic platform, the lower the  $\Delta E$ , the better the electron transfer ability of the electrode.<sup>41</sup> Thus the electron transfer ability of rPE (0.185 V) is better than PE (0.300 V), proving that the reduction of GO resulted in a higher electron transfer ability. Fig. 2c shows the CV curves of PE and rPE in 0.1 M phosphate buffer (PB, pH = 7) and 2 mM amitrole in 0.1 M PB at the scan rate of 50 mV s<sup>-1</sup>. As illustrated, there are redox peaks observed for amitrole both on the PE and rPE. Comparing with PE, the catalytic peak current of amitrole on the rPE is enhanced and the oxidation peak potential is slightly negatively shifted, proving that the reduction of GO has a catalytic effect on the detection of amitrole. Therefore, the rPE is selected as the working electrode in the following experiments.

### 3.2.2 Effect of pH variation of the supporting electrolyte.

The pH variation of the supporting electrolyte significantly alters the electrochemical oxidation of amitrole on the electrode surface.<sup>8</sup> The effect of pH on the current response of amitrole (2 mM) was evaluated using CV employing reduced paper electrode (rPE) over the pH range of 5–11. As shown in Fig. 3a, there is no obvious redox peak under acidic conditions while it was observed under neutral and alkaline conditions. The cyclic voltammogram in Fig. 3b can investigate the reduction and oxidation process of amitrole. When the applied voltage reaches +0.5 V (vs. Ag/AgCl), the amitrole will oxidize on the surface of

the rPE, and the current response will increase, forming an oxidation peak on the CV diagram. Similarly, when the voltage reaches about -0.1 V (vs. Ag/AgCl), the reductive reaction will occur, forming a reduction peak. The oxidation peak potential  $E_p$  is about +0.5 V (vs. Ag/AgCl), which is much lower than most electrocatalytic potential of modified electrode.<sup>41,42</sup> It was observed that the oxidation peak potential shifted slightly negatively as pH of the electrolyte was increased. Since the background current detected by rPE in PB is also affected by pH, we used the ratio of oxidation peak current  $I_p$  to background current  $I_0$  to evaluate the detection effect. Fig. 3c shows the effect of pH on oxidation peak current ( $I_p$ ) and the detection effect ( $I_p/I_0$ ). The experimental results show that optimum detection effect and high oxidation peak current were obtained at pH 9, suggesting the suitability for the detection of amitrole employing the reduced paper electrode.

### 3.2.3 Effect of scan rate variation and kinetic studies of amitrole.

Scan rate variation studies reveal the adsorption or diffusion mechanism,<sup>8</sup> reversibility of the electrocatalytic reactions of amitrole and kinetic parameters<sup>43</sup> at the reduced paper electrode at pH 9 by cyclic voltammetry (Fig. 4a). It is observed that the current response of background and amitrole increases with increasing scan rate ranging from 5 mV s<sup>-1</sup> to 500 mV s<sup>-1</sup>. To reduce the influence of background current, we used the ratio of oxidation peak current  $I_p$  to background current  $I_0$  to evaluate the detection effect. Comparing the oxidation peak current ( $I_p$ ) and detection effect ( $I_p/I_0$ ) shown in Fig. 4b, it is found that 100 mV s<sup>-1</sup> is the optimum scan rate.

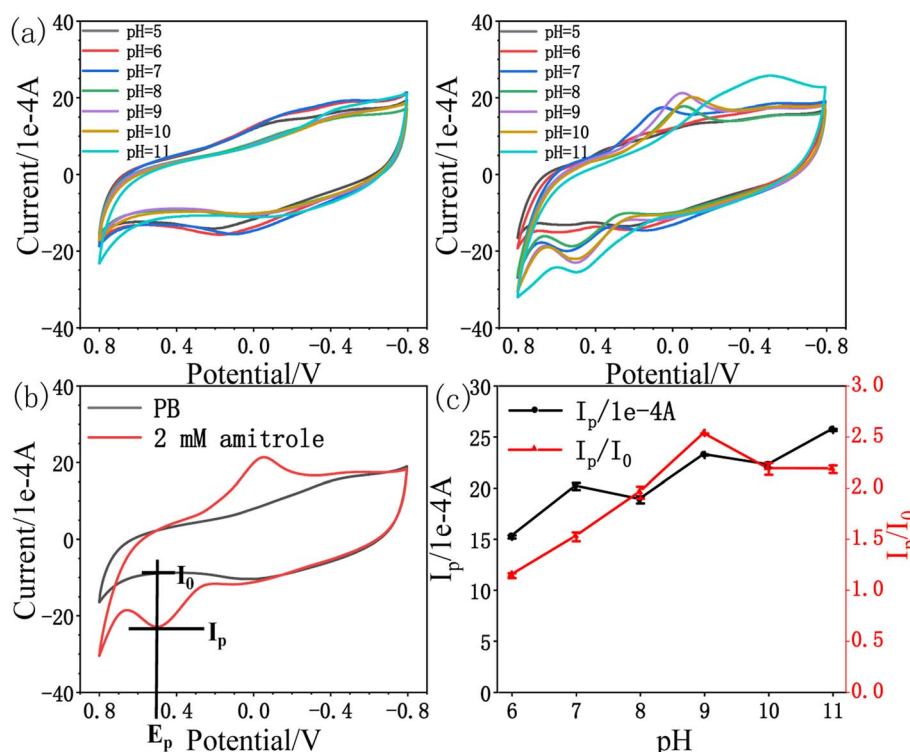


Fig. 3 (a) CVs of varying pH electrolyte at the scan rate of 50 mV s<sup>-1</sup>. The electrolyte: left is PB, right is 2 mM amitrole in PB. (b) CVs of PB and 2 mM amitrole in PB at the scan rate of 50 mV s<sup>-1</sup> and pH 9. (c) Plot of oxidation peak current ( $I_p/1 \times 10^{-4}$  A) and detection effect ( $I_p/I_0$ ) vs. pH.



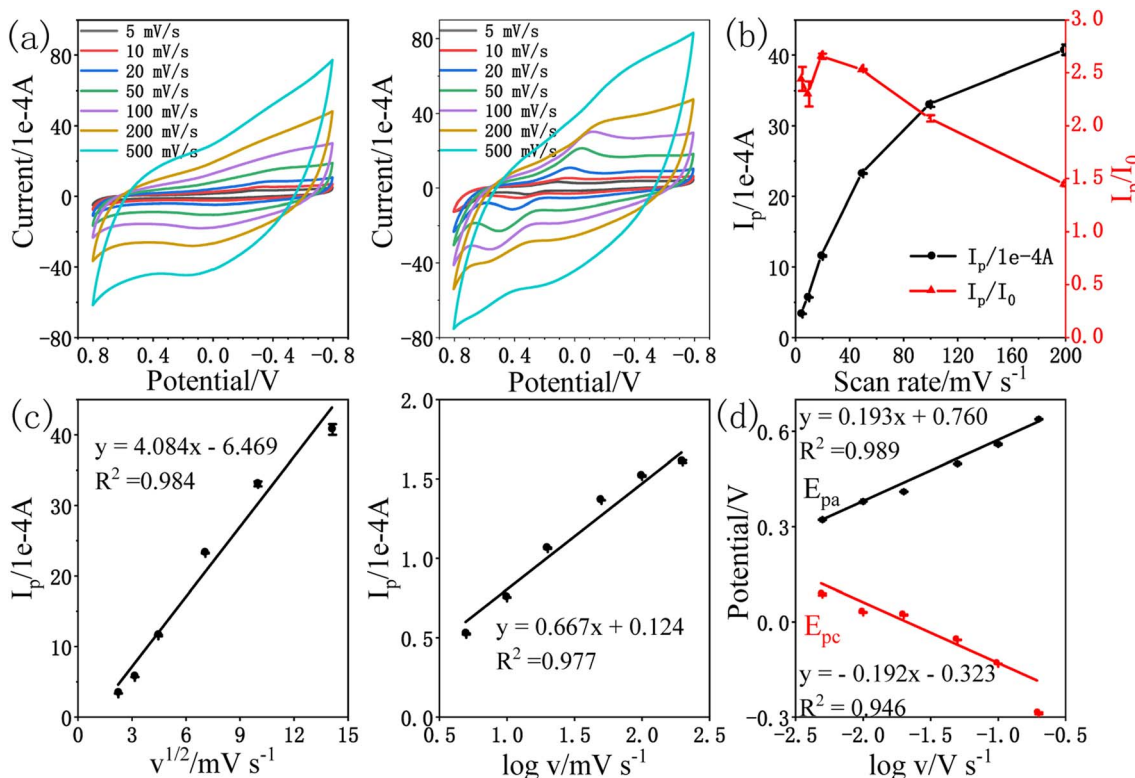


Fig. 4 (a) CVs of different scan rate values ( $5\text{--}500\text{ mV s}^{-1}$ ), the electrolyte ( $\text{pH} = 9$ ): left is PB, right is  $2\text{ mM}$  amitrole in PB. (b) Plot of oxidation peak current ( $I_p/1 \times 10^{-4}\text{ A}$ ) and detection effect ( $I_p/I_0$ ) vs. scan rate. (c) Plot of oxidation peak current ( $I_p/1 \times 10^{-4}\text{ A}$ ) vs. square root of the scan rate ( $v^{1/2}$ ); plot of logarithm of peak current ( $\log I_p/1 \times 10^{-4}\text{ A}$ ) vs. logarithm of scan rate ( $\log v/\text{mV s}^{-1}$ ). (d) Plot of peak potential ( $E_p/\text{V}$ ) vs. logarithm of scan rate ( $\log v/\text{V s}^{-1}$ ).

The obtained results exhibited that the oxidation peak current ( $I_p$ ) of amitrole followed a linear relationship with the square root of scan rate ( $v^{1/2}$ ) as indicated in Fig. 4c. The linear regression equation is shown below:

$$I_p (1 \times 10^{-4} \text{ A}) = 4.084v^{1/2} (\text{mV s}^{-1}) - 6.469; R^2 = 0.984$$

Further, the slope value of logarithm of  $I_p$  vs. logarithm of  $v$  was calculated to be 0.667 for amitrole, which is near to the

theoretical value as observed for the diffusion controlled processes,<sup>4,44</sup> confirming that the electrochemical process of amitrole on the surface of rPE is diffusion controlled.<sup>45</sup> The linear regression equation is shown below:

$$\log I_p (1 \times 10^{-4} \text{ A}) = 0.667 \log v (\text{mV s}^{-1}) + 0.124; R^2 = 0.977$$

Fig. 4d shows the anodic peak potential  $E_{\text{pa}}$  and the cathodic peak potential  $E_{\text{pc}}$  were proportional with the  $\log v$  with the

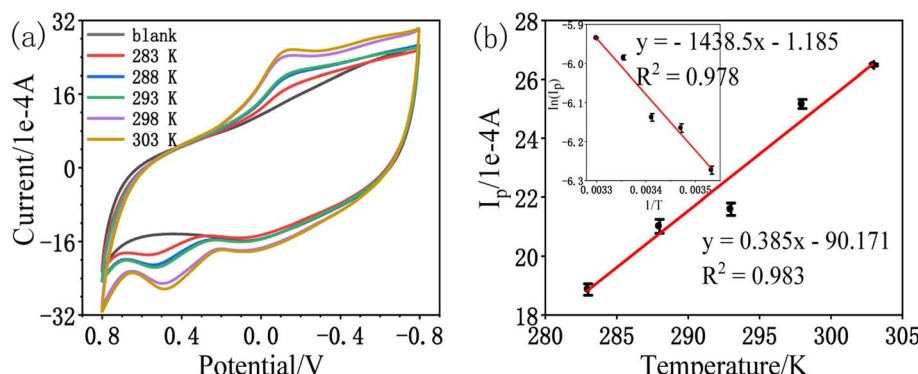


Fig. 5 (a) CVs of  $0.5\text{ mM}$  amitrole with respect to different temperature at rPE in  $\text{pH} 9$ , scan rate =  $100\text{ mV s}^{-1}$ . (b) Plot of oxidation peak current ( $I_p/1 \times 10^{-4}\text{ A}$ ) vs. temperature, inset: plot of  $\ln(I_p)$  vs.  $1/T$ .

linear regression equations as:  $E_{pa}$  (V) = 0.193  $\log v$  (V s<sup>-1</sup>) + 0.760 ( $R^2$  = 0.989) and  $E_{pc}$  (V) = -0.192  $\log v$  (V s<sup>-1</sup>) - 0.323 ( $R^2$  = 0.946), respectively. According to L伐iron's theory, the slopes of the lines are equal to  $2.3RT/(1 - \alpha)nF$  for the anodic peak and  $-2.3RT/\alpha nF$  for the cathodic peak, respectively.<sup>46,47</sup> The charge transfer coefficient  $\alpha$  can be calculated to be 0.50, indicating that the activated complex is at least halfway between substrate and the product on the reaction coordinate.<sup>17</sup> With the increase of scan rate, the oxidation peak potential gradually shifts positively and the reduction peak potential shifts negatively,

indicating that the electrochemical reaction of amitrole on the surface of rPE is a quasi-reversible reaction.<sup>48</sup>

**3.2.4 Effect of temperature.** The influence of temperature on the detection of amitrole was investigated by using CV technique on the reduced paper electrode at the scan rate of 100 mV s<sup>-1</sup>. With temperature increased from 283 K to 303 K, the oxidation peak current of amitrole increased linearly, as shown in Fig. 5. According to the thermodynamic eqn (2), the plot of  $\ln(I_p)$  vs. inverse temperature is determined to be relatively linear.

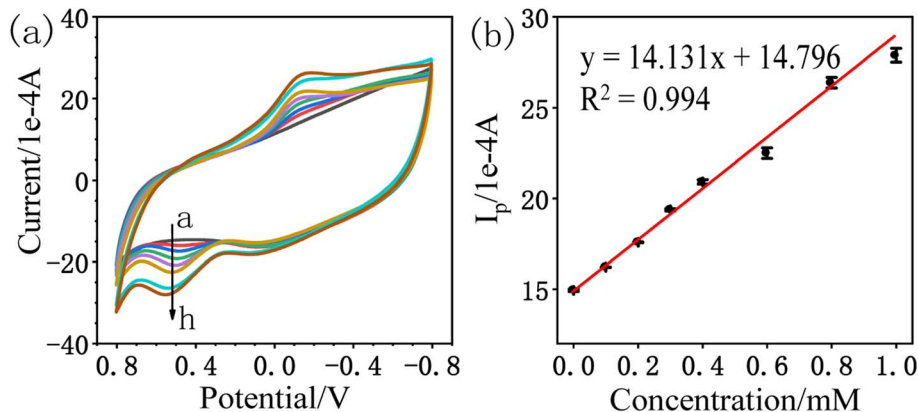


Fig. 6 (a) CVs of different concentration of amitrole at the scan rate of 100 mV s<sup>-1</sup> and pH 9: a-blank, b-0.1, c-0.2, d-0.3, e-0.4, f-0.6, g-0.8, h-1.0 mM. (b) Plot of oxidation peak current ( $I_p/1 \times 10^{-4}$  A) vs. amitrole concentration.

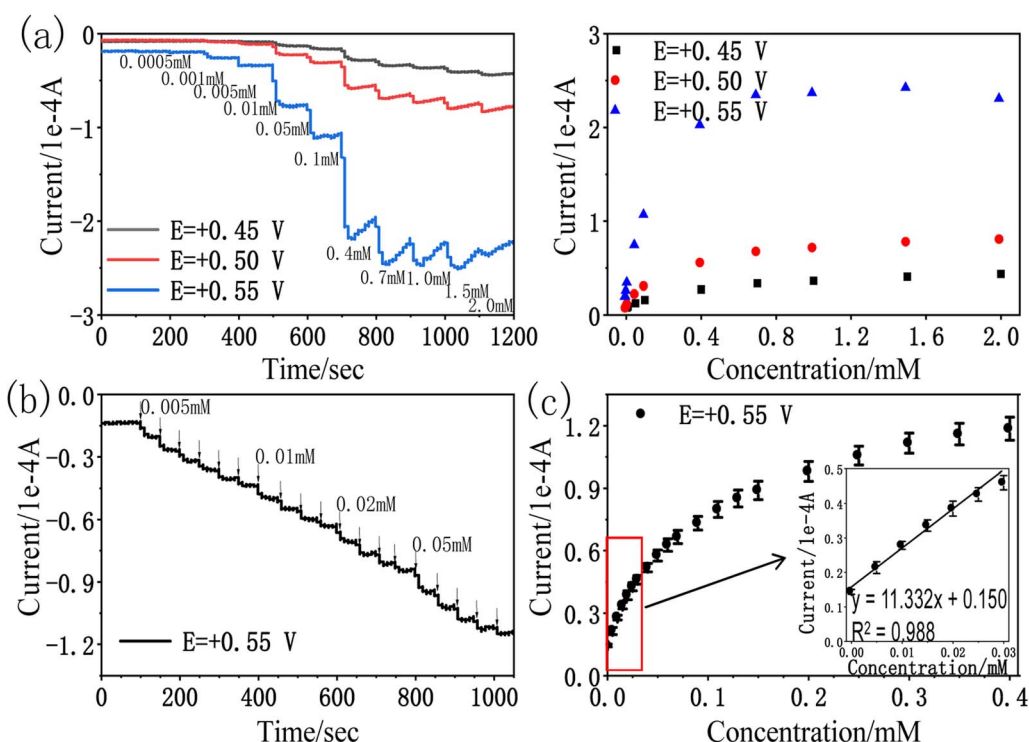


Fig. 7 (a) Amperometric response at reduced paper electrode kept at different applied potential (vs. Ag/AgCl) in PB (pH 9), with concentration in the range 0 mM to 2.0 mM; plot of current response vs. amitrole concentration. (b)  $I-t$  curve of amitrole concentrations ranging from 0 mM to 0.4 mM at applied potential +0.55 V. (c) Plot of amperometric current vs. amitrole concentration.



Table 1 Comparative study of LOD for amitrole with other reported methods

S. No.	Modified electrode	Method	Linearity range (μM)	LOD (M)	Ref.
1	GCE <sup>a</sup> /Nafion/lead-ruthenium oxide pyrochlore	SWV <sup>d</sup>	30–250	$3.8 \times 10^{-7}$	3
2	CPE <sup>b</sup> /iron(II) phthalocyanine nanoparticles	CA <sup>e</sup>	0.001–0.012	$3.62 \times 10^{-9}$	2
3	GCE/tetraaminophthalocyanine-single walled carbon nanotube dendrimer	CA	63–100	$2.15 \times 10^{-7}$	17
4	WO <sub>3</sub> ·0.33H <sub>2</sub> O/CPE	SWV	0.1–0.28	$2.30 \times 10^{-9}$	8
5	GCE/calcium cross linked pectin stabilized gold nanoparticle film	SWV	0.1–1.5	$2.0 \times 10^{-8}$	1
6	GCE/graphene oxide-MWCNTs <sup>c</sup>	<i>I</i> - <i>t</i> <sup>f</sup>	5–3545	$4.5 \times 10^{-7}$	25
7	GCE/calcium-doped zinc oxide nanoparticles-MWCNTs	SWV	0.01–0.6	$3.58 \times 10^{-9}$	5
8	GCE/N-doped carbon nanotube arrayed mesoporous carbon	DPV <sup>g</sup>	20–250	$7.0 \times 10^{-6}$	26
9	Carbon fibers/reduced graphene oxide/ cellulose paper	<i>I</i> - <i>t</i>	5–30	$2.44 \times 10^{-7}$	Present work

<sup>a</sup> GCE; glassy carbon electrode. <sup>b</sup> CPE; carbon paste electrode. <sup>c</sup> MWCNTs; multi-walled carbon nanotubes. <sup>d</sup> SWV; square-wave voltammetry. <sup>e</sup> CA; chronoamperometry. <sup>f</sup> *I*-*t*; amperometric *i*-*t*. <sup>g</sup> DPV; differential pulse voltammetry.

$$\begin{aligned} \sigma &= \sigma^0 e^{-\frac{E_a}{RT}} \\ D &= D^0 e^{-\frac{E_a}{RT}} \end{aligned} \quad (2)$$

where  $E_a$  is the activation energy,  $\sigma/D$ -conductivity/diffusibility,  $\sigma^0/D^0$ -standard conductivity/initial diffusibility,  $T$ -temperature in kelvin,  $R$ -universal gas constant.

The activation energy value of the oxidation peak current of amitrole is calculated from the Arrhenius equation to be  $11.96 \text{ kJ mol}^{-1}$ . Although the oxidation peak current is larger at higher temperature, this may be due to the diffusibility variations of the amitrole molecule.<sup>5,23</sup>

### 3.3. Electrochemical behaviour towards amitrole

**3.3.1 Concentration variation and detection limit of amitrole.** Cyclic Voltammetry (CV) was employed to detect varying concentration of amitrole using the reduced paper electrode with scan rate  $100 \text{ mV s}^{-1}$  at pH 9. As shown in Fig. 6, the oxidation peak potential  $E_p$  of amitrole is about  $+0.5 \text{ V}$  (vs. Ag/AgCl), and it is obvious that an orderly increase in the oxidation peak current  $I_p$  at increasing concentration. In the concentration range  $0.1 \text{ mM}$  to  $1.0 \text{ mM}$ , the  $I_p$  has a good linear relationship with the concentration, the regression equation of the linear plot is as follows:

$$I_p (1 \times 10^{-4} \text{ A}) = 14.131 C_A (\text{mM}) + 14.796; R^2 = 0.994$$

where  $C_A$  represents the concentration of amitrole. The limit of detection (LOD) is  $1.5 \times 10^{-5} \text{ mol L}^{-1}$  and sensitivity is  $1.41 \text{ mA mM}^{-1}$ . LOD is calculated from the calibration curve using the following equation:<sup>49</sup>  $\text{LOD} = 3\text{SD}/b$ . SD stands for the standard deviation of blank value (the corresponding anode current value of the CV curve scanned in PB at  $+0.5 \text{ V}$  was taken as blank value), and  $b$  is the slope of the linear regressive equation.

**3.3.2 Amperometric detection of amitrole at the reduced paper electrode.** Amperometric method<sup>50</sup> under stirred

conditions has a much higher current sensitivity than cyclic voltammetry, so it can be used to examine the sensitivity of the reduced paper electrode and the lower limit of detection of amitrole. Under the action of magnetic stirrer (rotation speed 80 rpm), which provides convective transmission,<sup>51</sup> the reduced paper electrode (rPE) was immersed in  $0.1 \text{ M}$  PB (pH = 9) solution and reacted for 2000 s to stabilize the background current. In order to explore the effect of applied potential, Fig. 7a shows the amperometric *I*-*t* curve obtained for amitrole at rPE in a homogeneously stirred PB at different applied potential (vs. Ag/AgCl), with concentration in the range  $0 \text{ mM}$  to  $2.0 \text{ mM}$ . It was found that when the potential is  $+0.55 \text{ V}$  (vs. Ag/AgCl), the current response of amitrole is obvious.

We further demonstrated the *I*-*t* curve of amitrole concentration in the range  $0 \text{ mM}$  to  $0.40 \text{ mM}$  under conditions at which the potential of rPE was kept at  $+0.55 \text{ V}$  vs. Ag/AgCl. Initially,  $0.005 \text{ mM}$  amitrole was added at a time, then gradually increased the concentration to  $0.01 \text{ mM}$ ,  $0.02 \text{ mM}$  and

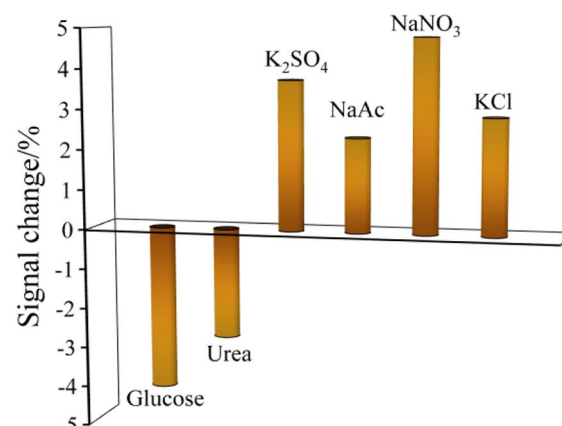


Fig. 8 Interference studies of ions and dissolved organic matters in the determination of amitrole by CV technique.



0.05 mM. Fig. 7b shows that during the successive addition of amitrole, typical current responses were observed. In the process of amperometric *I-t* detection, the increase rate of response current gradually decreases as the concentration of amitrole increases (Fig. 7c). This may be because the oxidized product was partially blocked on the paper electrode, leading to the reduction of its electrochemical activity and the decrease of sensitivity in the subsequent concentration detection.<sup>31,52,53</sup> As shown in inset of Fig. 7c, the amperometric current response was increased linearly with increasing amitrole concentration in the range 0.005 mM to 0.030 mM. The regression equation of the linear plot is shown as:

$$I (1 \times 10^{-4} \text{ A}) = 11.332C_A (\text{mM}) + 0.150; R^2 = 0.988$$

where *I* represents the current response, and *C<sub>A</sub>* represents the concentration of amitrole. The electroanalytical parameters such as LOD ( $2.44 \times 10^{-7}$  mol L<sup>-1</sup>, based on S/N = 3) and sensitivity (1.13 mA mM<sup>-1</sup>) were also evaluated from the above expression. Comparing the calculated values with the literature data in Table 1, the linear range and the low detection limit of the carbon fibers/reduced graphene oxide/cellulose paper electrode towards amitrole oxidation are comparable to other electrodes that require complex modifications.

## 4. Analytical applications

### 4.1. Interference studies

The selectivity of the reduced paper electrode towards amitrole was carried out using CV method. In the existence of 100 folds excess concentration (50 mM) of interfering ions and dissolved organic matters such as KCl, NaNO<sub>3</sub>, NaAc, K<sub>2</sub>SO<sub>4</sub>, urea, and glucose, it was seen from Fig. 8 that the above mentioned interferents did not show any significant effect (did not surpass  $\pm 5\%$ ) on the oxidation peak current of amitrole. The results suggested the reduced paper sensor has high selectivity in the detection of amitrole.

### 4.2. Analysis of amitrole in water samples

From *I-t* technique, the practical feasibility of the reduced paper sensor detection of amitrole was demonstrated in lake and tap water samples. First, filter paper was used to remove impurities and dust particles from the water sample. Then, pretreated water samples were prepared with corresponding concentrations of 0.01, 0.02 and 0.03 mM with standard amitrole solutions to study the recovery. The results of water samples evaluation are shown in Table 2. The recovery and relative standard deviation results proved that the reduced

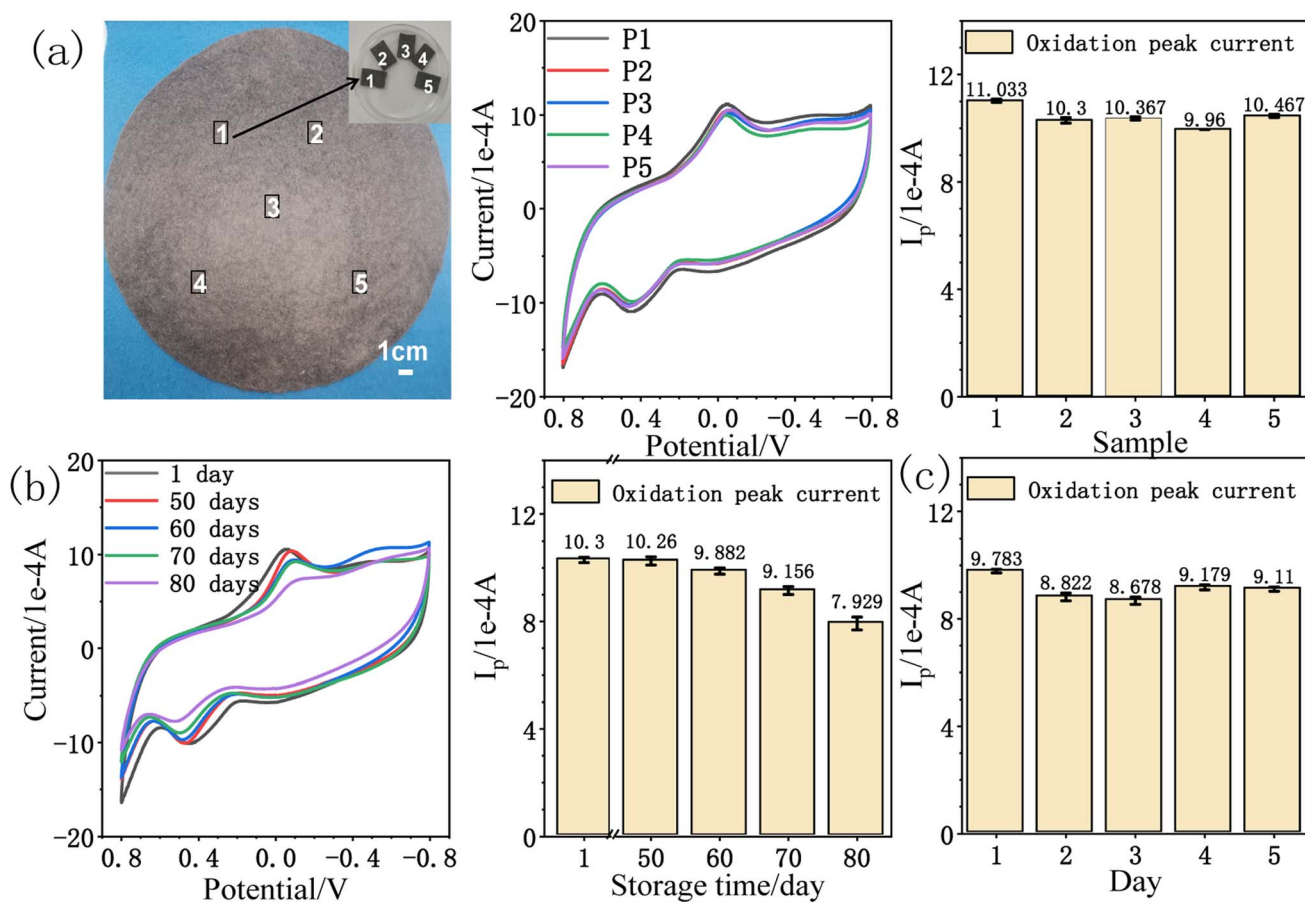


Fig. 9 (a) Reproducibility. CVs of 0.5 mM amitrole by five pieces of rPE taken from different locations of composite paper at a scan rate of 50 mV s<sup>-1</sup> and pH 9. (b) Storage stability. CVs and the oxidation peak current of 0.5 mM amitrole at a scan rate of 50 mV s<sup>-1</sup> and pH 9; The rPE were stored in the atmosphere for 80 days. (c) Repeatability. The oxidation peak current of 0.5 mM amitrole tested for five consecutive days.



Table 2 Detection of amitrole in water samples by *I-t* technique

Water samples	Added ( $10^{-4}$ M)	Detected ( $10^{-4}$ M)	Recovery (%)	RSD (%)
Tap water	0.1	0.1047	104.7	3.19
	0.2	0.2075	103.8	5.02
	0.3	0.3020	100.7	2.34
Lake water	0.1	0.1016	101.6	3.81
	0.2	0.2036	101.8	6.59
	0.3	0.3048	101.3	5.74

paper sensor has practicability in actual environmental samples.

#### 4.3. Stability and reproducibility

The reduced paper electrode has good current response effect and low detection limit towards amitrole detection. The repeatability<sup>54</sup> and stability<sup>28</sup> of rPE were investigated by cyclic voltammetry. As illustrated in Fig. 9a, five reduced paper electrodes were taken and tested in PB (pH = 9) solution containing 0.5 mM amitrole at a scan rate of 50 mV s<sup>-1</sup>. Stable and reproducible current responses for amitrole oxidation were obtained, the average oxidation peak current is  $10.43 \times 10^{-4}$  A with a relative standard deviation (RSD) of 3.74%, indicating that the inter-electrode reproducibility<sup>55</sup> of rPE is very good. To check the storage stability of rPE, it was stored in air at room temperature for 80 days. Fig. 9b shows the CVs and the oxidation peak current of 0.5 mM amitrole during this period. It was found that the current response for amitrole oxidation has reserved more than 95% of the initial value after 60 days. In addition, the CV curves in 0.5 mM amitrole solution for 5 consecutive days tested the repeatability of the electrocatalytic effect of the rPE. As shown in Fig. 9c, the RSD of the oxidation peak current was 4.68%, indicating that the measurement of the rPE can be used multiple times. These results demonstrate that the reduced paper electrode is an efficient and stable electrochemical sensor for amitrole analysis.

## 5. Conclusion

This study shows that paper-based electrodes prepared from carbon fibers (CF), reduced graphene oxide (rGO) and cellulose exhibit excellent performance in electrochemical detection of amitrole. Compared with traditional electrodes, the reduced paper electrode has certain advantages, such as easy fabrication, good reproducibility, storage stability and excellent catalytic activity. The paper electrode has good electrocatalytic performance for the oxidation of amitrole, showing low peak potential, high sensitivity, wide linear range and low detection limit, which is expected to realize the electrochemical detection of pesticides with portable, disposable, patterned paper-based electrodes. The sensitive electrochemical method can detect amitrole at the micro molar level, which is promising as an amperometry-based sensor to determine amitrole content in the field of food safety inspection and agricultural wastewater monitoring.

## Conflicts of interest

There are no conflicts of interest to declare.

## Acknowledgements

This work was financially supported by the National Key Research and Development Program of China (2019YFE0114400).

## References

- 1 V. Mani, R. Devasenathipathy, S. Chen, V. S. Vasantha, M. Ajmal Ali, S. Huang and F. M. A. Al-Hemaid, *Analyst*, 2015, **140**, 5764–5771.
- 2 M. Siswana, K. I. Ozoemena and T. Nyokong, *Talanta*, 2006, **69**, 1136–1142.
- 3 J. M. Zen, A. Senthil Kumar and M. R. Chang, *Electrochim. Acta*, 2000, **45**, 1691–1700.
- 4 D. Ilager, N. P. Shetti, K. R. Reddy, S. M. Tuwar and T. M. Aminabhavi, *Environ. Res.*, 2022, **204**, 111856.
- 5 S. J. Malode, K. Keerthi Prabhu and N. P. Shetti, *New J. Chem.*, 2020, **44**, 19376–19384.
- 6 G. Liu, J. Ling and J. Li, *ACS Sens.*, 2021, **6**, 4185–4192.
- 7 Y. Sun, P. F. Liu, D. Wang, J. Q. Li and Y. S. Cao, *J. Agric. Food Chem.*, 2009, **57**, 4540–4544.
- 8 D. Ilager, H. Seo, N. P. Shetti, S. S. Kalanur and T. M. Aminabhavi, *Sci. Total Environ.*, 2020, **743**, 140691.
- 9 W. Li, Y. Xue, X. Fu, Z. Ma and J. Feng, *Food Control*, 2022, **133**, 108587.
- 10 G. P. Danezis, C. J. Anagnostopoulos, K. Liapis and M. A. Koupparis, *Anal. Chim. Acta*, 2016, **942**, 121–138.
- 11 Y. Chu, Z. Tong, X. Dong, M. Sun, T. Gao, J. Duan and M. Wang, *Microchem. J.*, 2020, **156**, 104975.
- 12 M. Chicharro, A. Zapardiel, E. Bermejo and M. Moreno, *Talanta*, 2003, **59**, 37–45.
- 13 M. Chicharro, M. Moreno, E. Bermejo, S. Ongay and A. Zapardiel, *J. Chromatogr. A*, 2005, **1099**, 191–197.
- 14 F. Arduini, S. Cinti, V. Caratelli, L. Amendola, G. Palleschi and D. Moscone, *Biosens. Bioelectron.*, 2019, **126**, 346–354.
- 15 G. Han, J. Cai, C. Liu, J. Ren, X. Wang, J. Yang and X. Wang, *Appl. Surf. Sci.*, 2021, **541**, 148566.
- 16 M. Siswana, K. Ozoemena and T. Nyokong, *Sensors*, 2008, **8**, 5096–5105.
- 17 T. Mugadza and T. Nyokong, *Electrochim. Acta*, 2010, **55**, 2606–2613.
- 18 Y. Liu, E. Kim, J. Li, M. Kang, W. E. Bentley and G. F. Payne, *Nano Commun. Netw.*, 2017, **11**, 76–89.
- 19 X. Zhu, L. Lin, R. Wu, Y. Zhu, Y. Sheng, P. Nie, P. Liu, L. Xu and Y. Wen, *Biosens. Bioelectron.*, 2021, **179**, 113062.
- 20 T. E. Winkler, R. Dietrich, E. Kim, H. Ben-Yoav, D. L. Kelly, G. F. Payne and R. Ghodssi, *Electrochim. Commun.*, 2017, **79**, 33–36.
- 21 N. Elgrishi, K. J. Rountree, B. D. McCarthy, E. S. Rountree, T. T. Eisenhart and J. L. Dempsey, *J. Chem. Educ.*, 2018, **95**, 197–206.



22 D. Ilager, H. Seo, N. P. Shetti and S. S. Kalanur, *J. Environ. Chem. Eng.*, 2020, **8**, 104580.

23 S. J. Malode, K. Keerthi Prabhu, N. P. Shetti and K. R. Reddy, *Environ. Technol. Innovation*, 2021, **21**, 101222.

24 A. A. Ensafi, M. Amini and B. Rezaei, *Colloids Surf., B*, 2013, **109**, 45–51.

25 R. Devasenathipathy, *Int. J. Electrochem. Sci.*, 2017, **12**, 5888–5897.

26 S. Zhou, H. Xu, J. Liu, Y. Wei, X. Ma, Z. Han and H. Chen, *Chem. Phys.*, 2021, **542**, 111074.

27 A. W. Martinez, S. T. Phillips, M. J. Butte and G. M. Whitesides, *Angew. Chem., Int. Ed.*, 2007, **46**, 1318–1320.

28 C. Wang, R. Wu, H. Ling, Z. L. Zhao, W. J. Han, X. W. Shi, G. F. Payne and X. H. Wang, *npj Flexible Electron.*, 2022, **6**, 1–8.

29 D. Jemmeli, E. Marcoccio, D. Moscone, C. Dridi and F. Arduini, *Talanta*, 2020, **216**, 120924.

30 J. Bhardwaj, S. Devarakonda, S. Kumar and J. Jang, *Sens. Actuators, B*, 2017, **253**, 115–123.

31 W. Kit-Anan, A. Olarnwanich, C. Sriprachuabwong, C. Karuwan, A. Tuantranont, A. Wisitsoraat, W. Srituravanich and A. Pimpin, *J. Electroanal. Chem.*, 2012, **685**, 72–78.

32 T. Wang, R. C. Reid and S. D. Minteer, *Electroanal.*, 2016, **28**, 854–859.

33 T. Li, C. Chen, A. H. Brozena, J. Y. Zhu, L. Xu, C. Driemeier, J. Dai, O. J. Rojas, A. Isogai, L. Wågberg and L. Hu, *Nature*, 2021, **590**, 47–56.

34 Y. Wang, J. Luo, J. Liu, S. Sun, Y. Xiong, Y. Ma, S. Yan, Y. Yang, H. Yin and X. Cai, *Biosens. Bioelectron.*, 2019, **136**, 84–90.

35 M. Kang, E. Kim, T. E. Winkler, G. Banis, Y. Liu, C. A. Kitchen, D. L. Kelly, R. Ghodssi and G. F. Payne, *Biosens. Bioelectron.*, 2017, **95**, 55–59.

36 K. Rahbar Shamskar, H. Heidari and A. Rashidi, *Ind. Crop. Prod.*, 2016, **93**, 203–211.

37 P. Ren, D. Yan, X. Ji, T. Chen and Z. Li, *Nanotechnology*, 2011, **22**, 55705.

38 X. Mei and J. Ouyang, *Carbon*, 2011, **49**, 5389–5397.

39 S. J. Dong and Z. Jin, *Electrochim. Acta*, 1989, **34**, 963–968.

40 J. J. Gooding, V. G. Praig and E. A. H. Hall, *Anal. Chem.*, 1998, **70**, 2396–2402.

41 P. T. Mafuwe, M. Moyo, T. Mugadza, M. Shumba and S. Nyoni, *J. Solid State Electrochem.*, 2019, **23**, 285–294.

42 A. Maringa, T. Mugadza, E. Antunes and T. Nyokong, *J. Electroanal. Chem.*, 2013, **700**, 86–92.

43 P. K. Kalambate, B. J. Sanghavi, S. P. Karna and A. K. Srivastava, *Sens. Actuators, B*, 2015, **213**, 285–294.

44 U. S. Aithal and T. M. Aminabhavi, *J. Chem. Educ.*, 1990, **67**, 82–85.

45 M. Chicharro, A. Arribas, M. Moreno, E. Bermejo and A. Zapardiel, *Talanta*, 2007, **74**, 376–386.

46 W. Zhu, H. Huang, X. Gao and H. Ma, *Mater. Sci. Eng., C*, 2014, **45**, 21–28.

47 E. Laviron, *J. Electroanal. Chem.*, 1979, **101**, 19–28.

48 S. Corona-Avendaño, G. Alarcón-Angeles, M. T. Ramírez-Silva, G. Rosquete-Pina, M. Romero-Romo and M. Palomar-Pardavé, *J. Electroanal. Chem.*, 2007, **609**, 17–26.

49 M. Brycht, K. Kaczmarska, B. Uslu, S. A. Ozkan and S. Skrzypek, *Diamond Relat. Mater.*, 2016, **68**, 13–22.

50 A. Salimi and K. Abdi, *Talanta*, 2004, **63**, 475–483.

51 S. G. Wang, Q. Zhang, R. Wang and S. F. Yoon, *Biochem. Biophys. Res. Commun.*, 2003, **311**, 572–576.

52 M. Gocyla, M. Pisarek, M. Holdynski and M. Opallo, *Electrochem. Commun.*, 2018, **96**, 77–82.

53 Q. He, S. Wu, Z. Yin and H. Zhang, *Chem. Sci.*, 2012, **3**, 1764–1772.

54 W. Huang, *Talanta*, 2003, **61**, 411–416.

55 A. Salimi and R. Hallaj, *J. Solid State Electrochem.*, 2012, **16**, 1239–1246.

